Magnetic excitations in magnetization plateaus of a frustrated spin ladder

Kota Sasaki,* Takanori Sugimoto,† and Takami Tohyama
Department of Applied Physics, Tokyo University of Science, Katsushika, Tokyo 125-8585, Japan

Shigetoshi Sota
Computational Materials Science Research Team, RIKEN Center for Computational Science, Kobe, Hyogo 650-0047, Japan

(Received 8 December 2019; accepted 10 March 2020; published 6 April 2020)

Magnetization plateaus emerging in quantum spin systems due to spontaneously breaking of translational symmetry have been reported both theoretically and experimentally. The broken symmetry can induce reconstruction of elementary excitations such as Goldstone and Higgs modes, whereas its microscopic mechanism and reconstructed quasiparticle in magnetization-plateau phases have remained unclear so far. Here we theoretically study magnetic excitations in the magnetization-plateau phases of a frustrated spin ladder by using the dynamical density-matrix renormalization-group method. Additionally, analytical approaches with the perturbation theory are performed to obtain an intuitive view of magnetic excitations. A comparison between numerical and analytical results indicates the presence of a reconstructed quasiparticle originating from spontaneously broken translational symmetry, which is realized as a collective mode of the spin trimer called a trimeron.

DOI: 10.1103/PhysRevB.101.144407

I. INTRODUCTION

Various quantum spin systems with frustration have been extensively studied, motivated by exotic characters such as the quantum spin liquid at zero temperature and quantization of magnetization with spontaneously broken translational symmetry. Actually, gapless quantum spin liquid states and gapped quantized states of magnetization have been reported not only theoretically but experimentally [1–4]. These states are often induced by frustration and are switchable by applied magnetic field. For example, the zigzag spin chain, where geometrical frustration originates from antiferromagnetic first- and second-neighbor interactions, is known as a typical quantum spin system exhibiting a gapped-to-gapless transition induced by magnetic field at zero temperature [5].

Compared with the ground-state properties, dynamical behaviors in magnetic fields have mostly not been clarified so far. In particular, dynamical properties in the quantized state of magnetization, the so-called magnetization plateau (MP) state, mostly remains unclear, despite the possible emergence of novel elementary excitations due to spontaneous symmetry breaking. In fact, recent studies on a weakly coupled spin-ladder compound reported a Higgs mode due to spontaneously broken symmetries [6–8]. Furthermore, these dynamical behaviors are crucial for understanding spin or heat transport, which is applicable to spintronics devices [9,10].

In this paper, we focus on magnetic excitations in a frustrated spin ladder (FSL), where antiferromagnetic interactions are assigned to the first- and second-neighbor bonds in a leg and the first-neighbor bond in a rung. This model exhibits three MPs at normalized finite magnetization $m \equiv M/M_{\rm sat} = 1/3,\ 1/2$, and $2/3$ with saturation magnetization $M_{\rm sat}$ [11,12]. Interestingly, all of these MPs are induced by spontaneously breaking translational symmetry, so that the MPs exhibit extended magnetic unit cells that are different from the original unit cell of this model. In addition, this model is regarded as an effective spin model to reproduce magnetic behaviors in real materials $BiCu_2PO_6$ [13–16] and $Li_2Cu_2O(SO_4)_2$ [17–20]. Actually, in $BiCu_2PO_6$, external field dependences [21–24], dynamical properties [25,26], and thermal conductivity [27–29] observed experimentally have been theoretically explained in the FSL model [30–32], although additional terms such as the Dzyaloshinskii-Moriya interaction are required to obtain a quantitative coincidence [33,34]. Therefore, the FSL model deserves to be investigated in terms of the relation between low-energy excitations and spontaneously broken symmetries of MP phases.

The preceding studies on the MP states [11,12] have presented the equivalence of two different models, the FSL in the strong-rung limit and an anisotropic frustrated spin chain (AFSC). According to these studies, the $m = 1/3,\ 1/2$, and $2/3$ MP states in the FSL correspond to $m' = -1/3$, 0, and $1/3$ MP states in the AFSC, respectively. Since the $m' = -1/3$ and $m' = 1/3$ MP states in the AFSC are connected to each other via a spin-flip pair, the corresponding $m = 1/3$ MP and $m = 2/3$ states in the FSL should have a common origin. Therefore, the dynamics of the $m = 1/3$ MP state is expected to be equivalent to that of the $m = 2/3$ MP state, while the $m = 1/2$ MP state can show qualitatively different dynamics.

We perform numerical calculations of the dynamical spin structure factor (DSSF) by using the dynamical density-matrix renormalization-group (DDMRG) method [35–38] to clarify the difference in dynamics in the $m = 1/3,\ 1/2$, and $2/3$ MP states for the FSL in the strong-rung limit. The dynamical

*1517617@alumni.tus.ac.jp
†sugimoto.takanori@rs.tus.ac.jp

behaviors of the $m' = 0$ and $1/3$ MP states in the AFSC are also examined in comparison with the dynamics of the FSL. The AFSC is useful for intuitive understanding of dynamical properties because of its simplicity. Moreover, a perturbative clusterization approach imposing spontaneously breaking of translational symmetry is used to obtain intuitive physical pictures of spin dynamics.

The contents of this paper are as follows. In Sec. II, we introduce the model Hamiltonians of the FSL and the AFSC. The equivalence of the two different models is briefly reviewed with a projection operator to low-lying states in the strong-rung limit of the FSL. We also introduce the DSSFs and model parameters for calculation. In Sec. III, the DSSFs obtained with the DDMRG are shown for three MP states in the FSL and two MP states in the AFSC. Section IV is used to give a qualitative explanation of characteristic structures in the DSSFs and an intuitive physical picture of spin dynamics. For this purpose, we introduce a perturbative clusterization approach imposing spontaneously breaking of translational symmetry. Finally, we summarize our results in Sec. V.

II. MODEL AND METHOD

In this section, we introduce two model Hamiltonians: the FSL and its corresponding model in the strong-rung limit, the AFSC. Additionally, the DSSFs that we calculate to investigate dynamical properties are defined.

A. Frustrated spin ladder

The Hamiltonian of the FSL is defined as

$$\mathcal{H} = \mathcal{H}_\perp + \mathcal{H}_\parallel + \mathcal{H}_Z, \tag{1}$$

with

$$\mathcal{H}_\perp = J_\perp \sum_{i=1}^{N} \boldsymbol{S}_{i,1} \cdot \boldsymbol{S}_{i,2}, \tag{2}$$

$$\mathcal{H}_\parallel = \sum_{\eta=1,2} J_\eta \sum_i \sum_{j=1,2} \boldsymbol{S}_{i,j} \cdot \boldsymbol{S}_{i+\eta,j}, \tag{3}$$

$$\mathcal{H}_Z = -H \sum_i \sum_{j=1,2} S^z_{i,j}, \tag{4}$$

where $\boldsymbol{S}_{i,1}$ ($\boldsymbol{S}_{i,2}$) is the $S = 1/2$ spin operator on the ith rung in the upper (lower) chain. Exchange energies of the first-neighbor bond in a leg, the second-neighbor bond in a leg, and the first-neighbor bond in a rung are denoted by J_1, J_2, and $J_\perp$, respectively. The magnitude of magnetic field is represented by H. In this paper, we focus on the strong-rung region of the FSL because three MPs at $m = 1/3$, $1/2$, and $2/3$ become robust in this limit. Moreover, this limit enables us to map the FSL to the AFSC, which is used to obtain an intuitive picture of dynamical behaviors.

B. The effective model of an FSL: AFSC

The Hamiltonian of the AFSC is given by the bond-operator (quasispin) transformation [11,12,39,40]. To obtain the AFSC Hamiltonian with quasispin operators, we use the basis of singlet and triplet states on the ith rung:

$$|s\rangle_i = \frac{1}{\sqrt{2}}(|\uparrow\rangle_{i,1}|\downarrow\rangle_{i,2} - |\downarrow\rangle_{i,1}|\uparrow\rangle_{i,2}), \tag{5}$$

$$|t^+\rangle_i = |\uparrow\rangle_{i,1}|\uparrow\rangle_{i,2}, \tag{6}$$

$$|t^0\rangle_i = \frac{1}{\sqrt{2}}(|\uparrow\rangle_{i,1}|\downarrow\rangle_{i,2} + |\downarrow\rangle_{i,1}|\uparrow\rangle_{i,2}), \tag{7}$$

$$|t^-\rangle_i = |\downarrow\rangle_{i,1}|\downarrow\rangle_{i,2}. \tag{8}$$

For simplicity, we call the $|t^\alpha\rangle_i$ ($\alpha = +, 0, -$) state the "α triplet" in the following. The Hamiltonian $\mathcal{H}$ (1) is rewritten with these bases.

In the strong-rung limit, leg interactions in $\mathcal{H}_\parallel$ (3) are regarded as perturbative terms. For $\mathcal{H}_\parallel = 0$, magnetization M jumps from zero to saturation magnetization $M_{\rm sat}$ at critical magnetic field $H_c = J_\perp$. Finite contributions from $\mathcal{H}_\parallel$ change the magnetization jump into a continuous curve including plateaus around the critical field. The range of field ΔH for partially magnetized states approximately equals $\Delta H \sim J_\parallel$. In this field region, the 0 and $-$ triplets are much higher in energy than the $+$ triplet. Therefore, we can ignore the 0 and $-$ triplets and thus obtain a low-energy effective Hamiltonian. To abandon the high-energy triplets, we introduce the projection operator $\mathcal{P} = \prod_i (|s\rangle_i\langle s|_i + |t^+\rangle_i\langle t^+|_i)$. The effective Hamiltonian is given by

$$\mathcal{H}' = \mathcal{P}\mathcal{H}\mathcal{P} = \sum_{\eta=1,2}\sum_i \frac{J_\eta}{2}\left(T_i^+ T_{i+\eta}^- + T_i^- T_{i+\eta}^+ + T_i^z T_{i+\eta}^z\right) - H' \sum_i T_i^z + \text{const}, \tag{9}$$

where spin-1/2 quasispin operators at site i are denoted by $\boldsymbol{T}_i$, given by $T_i^+ = |t^+\rangle_i\langle s|_i$, $T_i^- = |s\rangle_i\langle t^+|_i$, and $T_i^z = |t^+\rangle_i\langle t^+|_i - 1/2$. The effective magnetic field H' is defined by $H' = H - J_\perp - (J_1 + J_2)/2$. The effective Hamiltonian (9) describes the AFSC. Note that the z component of quasispin is given by $T_i^z = |t^+\rangle_i\langle t^+|_i - 1/2$. This leads to the relation where a normalized magnetization $m' \equiv M'/M'_{\rm sat} = 2m - 1$, with M' ($M'_{\rm sat}$) being magnetization (saturation magnetization) in the quasispin system. For example, $m = 1/3$, $1/2$, and $2/3$ in the FSL correspond to $m' = -1/3$, 0, and $1/3$ in the AFSC, respectively.

C. Dynamical spin structure factor

To investigate magnetic excitations of the FSL, we calculate the DSSF defined by

$$S^\pm(\boldsymbol{q}, \omega) = -\frac{1}{\pi}\text{Im}\,\langle\psi_0|\, S_{\boldsymbol{q}}^\mp \frac{1}{\omega - \mathcal{H} + E_0 + i\gamma} S_{\boldsymbol{q}}^\pm\, |\psi_0\rangle, \tag{10}$$

where $|\psi_0\rangle$ is the ground state, E_0 is the ground-state energy, and γ is an infinitesimal value. The Fourier component $S_{\boldsymbol{q}}^\pm$ under the open boundary condition is given by

$$S_{\boldsymbol{q}}^\pm = \sqrt{\frac{2}{N+1}} \sum_i \sin(q_x i) S_{i,q_y}^\pm, \tag{11}$$

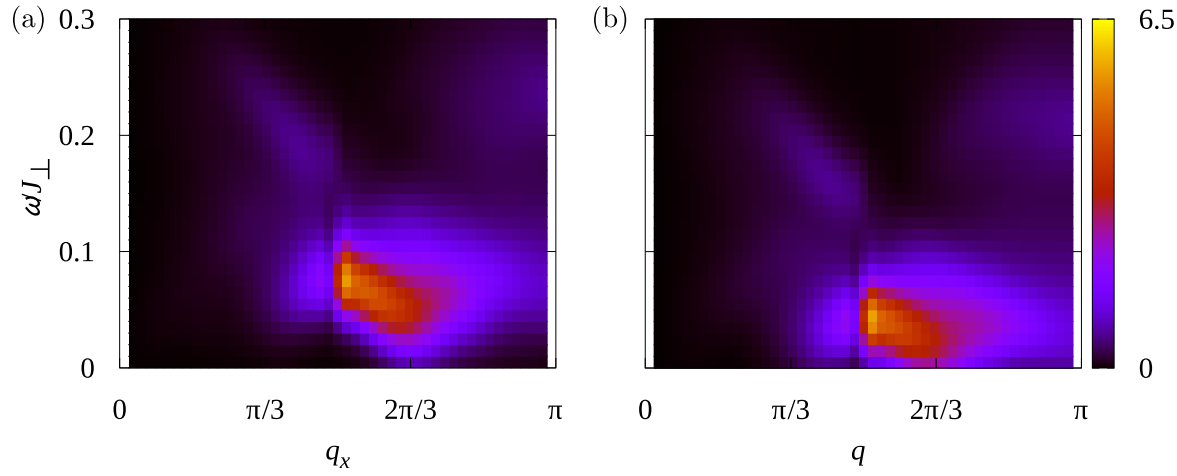

FIG. 1. (a) $S^+(q_x,\omega)$ in the $m=1/2$ MP phase of the FSL. (b) $T^+(q_x,\omega)$ in the $m'=0$ MP phase of AFSC. A broad excitation with minimum-energy excitations around $q_x=2\pi/3$ and an intensive peak at $q_x=\pi/2$ are common in (a) and (b).

with

$$S^{\pm}_{i,q_y=0}=\frac{1}{\sqrt{2}}(S^{\pm}_{i,1}+S^{\pm}_{i,2}),\quad S^{\pm}_{i,q_y=\pi}=\frac{1}{\sqrt{2}}(S^{\pm}_{i,1}-S^{\pm}_{i,2}), \tag{12}$$

where $S^{\pm}_{i,j}=S^{x}_{i,j}\pm iS^{y}_{i,j}$ and the wave number of the leg (rung) direction is given by $q_x=\frac{\pi}{N+1}n$ $(q_y=0,\pi)$, with $n=1,2,\ldots,N$, with N being the total number of rungs along the leg direction.

Similarly, the DSSF for the AFSC denoted by $T^{\pm}(q,\omega)$ is given by substituting the quasispin operator $T^{\pm}_q$ and $\mathcal{H}'$ for $S^{\pm}_{\boldsymbol{q}}$ and $\mathcal{H}$, respectively, in Eq. (10). Here $T^{\pm}_q=\sqrt{\frac{2}{N+1}}\sum_i \sin(qi)T^{\pm}_i$, and $q=\frac{\pi}{N+1}n$, with $n=1,2,\ldots,N$, with N being the total number of sites in the chain.

To obtain the DSSF numerically, we use the DDMRG method [36,37]. This method requires three target states, $|\psi_0\rangle$, $S^{\pm}_{\mathbf{q}}|\psi_0\rangle$, and $[\omega-\mathcal{H}+E_0+i\gamma]^{-1}S^{\pm}_{\mathbf{q}}|\psi_0\rangle$. The correction vector $[\omega-\mathcal{H}+E_0+i\gamma]^{-1}S^{\pm}_{\mathbf{q}}|\psi_0\rangle$ is obtained with the kernel-polynomial expansion method [38]. In this method, a Gaussian broadening with a width σ is introduced instead of Lorentzian broadening in Eq. (10).

III. RESULT

$S^{\pm}_{\boldsymbol{q}}$ in Eq. (11) has two modes, $q_y=0$ and $q_y=\pi$, with respect to rung parity. These two modes in Eq. (12) are rewritten by using the singlet and triplet bases:

$$S^{\pm}_{i,q_y=0}=|t^{\pm}\rangle_i\langle t^0|_i+|t^0\rangle_i\langle t^{\mp}|_i\,, \tag{13}$$

$$S^{\pm}_{i,q_y=\pi}=-(|t^{\pm}\rangle_i\langle s|_i+|s\rangle_i\langle t^{\mp}|_i). \tag{14}$$

Since the 0 triplet $|t^0\rangle_i$ in plateau regions is much higher in energy than the singlet $|s\rangle_i$ in the strong-rung limit, only the $q_y=\pi$ mode is enough to describe elementary excitations in the low-energy region. We thus discuss only the $q_y=\pi$ mode in this paper and abbreviate $S^{\pm}(q_x,q_y=\pi,\omega)$ for the FSL to $S^{\pm}(q_x,\omega)$ hereafter.

In our calculations, we use the following parameters: $J_1/J_\perp=0.2$ and $J_2/J_1=0.65$ in the 48-rung FSL and $\sigma=0.02J_\perp$. These parameters are chosen for the following reasons. First, in the real material $BiCu_2PO_6$, preceding studies have concluded that two spins on each rung form a singlet at low temperatures; that is, the ground state without magnetic fields is the so-called rung-singlet state [25,26,30,31]. The strong-rung condition $J_1/J_\perp=0.2$ also belongs to the rung-singlet phase, and we can apply perturbation analysis based on the strong-rung limit to clarify an intuitive physical picture of elementary excitations. Additionally, to stabilize the $m=1/3$, $1/2$, and $2/3$ MPs, we introduce the frustration $J_2/J_1=0.65$. In fact, we have confirmed that the MPs emerge due to spontaneously breaking symmetry [see Fig. 6(a) in Appendix A]. The system size, $N=48$ rungs, is sufficient to discuss dynamical behaviors at least qualitatively. With these parameters, the truncation error in DDMRG is less than 10^{-4} with 600 states kept in the DDMRG calculations.

A. S^+ excitation in the $m=\frac{1}{2}$ MP phase

Figure 1(a) shows $S^+(q_x,\omega)$ in the $m=1/2$ MP phase [for MP see Fig. 6(a) in Appendix A]. A broad but intensive peak centered at $\omega/J_\perp=0.08$ is seen at $q_x=\pi/2$. Its peak width is wider than the Gaussian width σ, indicating intrinsic broadening of the peak. We consider that this peak originates from a dimerized ground state in the $m=1/2$ MP phase, which breaks the translational symmetry spontaneously [11] and causes a doubled period of lattice. A broad but dispersive structure extends above $q_x=\pi/2$ with minimum-energy excitations around $q_x=2\pi/3$. This structure indicates multispinon excitation, and thus, we consider it a manifestation of fractionalized excitation with strong quantum fluctuation. In fact, the ground state of the $m=1/2$ MP in the FSL corresponds to the dimer state of the $m'=0$ MP in the AFSC, and thus, we can interpret the broad excitation as multispinons in the AFSC [41]. To confirm this interpretation, we calculate the DSSF of AFSC $T^+(q,\omega)$ in the $m'=0$ MP phase [see Fig. 1(b)]. We find similar structures in Fig. 1(b) compared with those in Fig. 1(a): a broad excitation with minimum energy excitations around $q_x=2\pi/3$ and an intensive peak at $q_x=\pi/2$. Therefore, we conclude that low-energy excitations

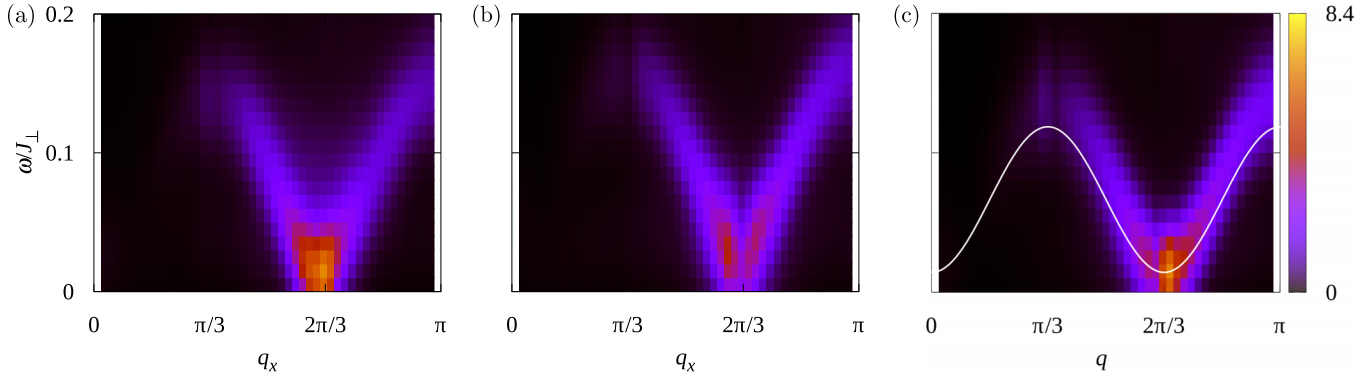

FIG. 2. (a) $S^-(q_x, \omega)$ in the $m = 1/3$ MP phase of the FSL. (b) $S^+(q_x, \omega)$ in the $m = 2/3$ MP phase of the FSL. (c) $T^+(q_x, \omega)$ in the $m' = 1/3$ MP phase of the AFSC. The white line shows the dispersion relation obtained by an analytical calculation assuming clusterization (see Sec. IV).

are due to multiple quasispinon excitations, including the intensive peak caused by the doubled period of lattice.

B. S^- (S^+) excitation in the $m = \frac{1}{3}$ ($\frac{2}{3}$) MP phase

$S^-(q_x, \omega)$ in the $m = 1/3$ MP phase and $S^+(q_x, \omega)$ in the $m = 2/3$ MP phase are shown in Figs. 2(a) and 2(b), respectively. These two spectra show a similar behavior with a dispersive feature with zero-energy excitation at $q_x = 2\pi/3$, indicating a period with three times the original unit-cell length in real space. This similarity is actually expected from the fact that both the $m = 1/3$ and $m = 2/3$ MPs can be associated with the array of quasispinons and share a common origin [11]. Since the $m = 2/3$ MP corresponds to the $m' = 1/3$ MP, the DSSF of the ASFC $T^+(q, \omega)$ in the $m' = 1/3$ MP phase also shows a similar dispersive feature with zero-energy excitation at $q_x = 2\pi/3$, as shown in Fig. 2(c) [42]. Based on the similarity, we may construct an intuitive view of spin dynamics via full examination of $T^+(q, \omega)$ in the $m' = 1/3$ MP phase. We will discuss this view in Sec. IV using a clusterization approach.

C. S^+ (S^-) excitation in the $m = \frac{1}{3}$ ($\frac{2}{3}$) MP phase

Figures 3(a) and 3(b) show $S^+(q_x, \omega)$ in the $m = 1/3$ MP phase and $S^-(q_x, \omega)$ in the $m = 2/3$ MP phase, respectively. These two figures share common features: two dispersive low-energy ($\omega/J_\perp < 0.3$) excitations with the minimum-energy excitation at $q_x = 2\pi/3$ and high-energy broad excitations at $\omega/J_\perp > 0.3$. We find that $T^-(q, \omega)$ in the $m' = 1/3$ MP phase shown in Fig. 3(c) exhibits spectral distributions similar to those in Figs. 3(a) and 3(b). To understand the origin of the spectra, we will introduce a clusterization approach for $T^-(q, \omega)$ in Sec. IV.

IV. DISCUSSION

Our purpose in this section is to give an intuitive physical view of elementary excitations in the $m = 1/3$ and $2/3$ MP phases using an analytical approach. The following discussion is based on spontaneous translational symmetry breaking in the MP phases, where the magnetic unit cell is larger than the original unit cell. In such a case, quantum entanglement between the magnetic unit cells is expected to be suppressed because of the enlargement of the unit cell. Therefore,

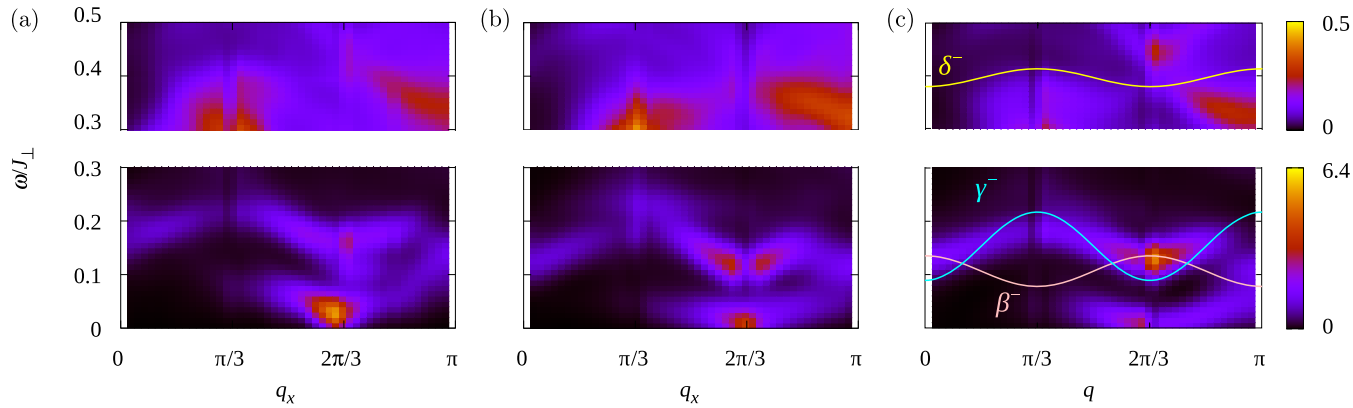

FIG. 3. (a) $S^+(q_x, \omega)$ in the $m = 1/3$ MP phase of the FSL. (b) $S^-(q_x, \omega)$ in the $m = 1/3$ MP phase of the FSL. (c) $T^-(q_x, \omega)$ in the $m' = 1/3$ MP phase of the AFSC. Each plot is split into upper and lower panels to make the distribution of the spectrum visible. In (c), the pink line shows the dispersion of the β^- excitation obtained by an analytical calculation assuming clusterization (see Sec. IV). The blue and yellow lines show the dispersion relations of γ^- and δ^-, respectively.

effective interactions between the enlarged unit cells can be approximated to a semiclassical one (see Appendix B). If the interactions are totally classical, the ground state is given by the direct product of local quantum states, which are obtained by exact diagonalization of the local Hamiltonian in the enlarged unit cell. Such a local quantum state contributing to the ground state should be one of low-lying states in the local Hamiltonian. Otherwise, the intercell interactions will become larger than intracell interaction, contradicting the localized nature of spins in the magnetic unit cell. Even in the case of semiclassical interactions where the ground state becomes a superposition of the direct product of local states, the local states contributing to the ground state should be low-lying states. Based on this reasoning, we restrict the Hilbert space of the enlarged unit cell to several low-lying states obtained by exact diagonalization of the local Hamiltonian. Moreover, the interactions between the enlarged unit cells are projected onto the restricted Hilbert space. We call this approach a clusterization based on spontaneously broken symmetry (CBSBS).

In the following, we apply the CBSBS to the $m' = 1/3$ MP phase in the AFSC because magnetic excitations in the $m = 1/3$ and $2/3$ MP phases of the FSL are qualitatively similar to the $T^{\pm}$ excitations in the $m' = 1/3$ MP phase of the AFSC (see Sec. III). The magnetic unit cell is enlarged to three times longer than the original one due to spontaneous translational symmetry breaking. Therefore, we use the following Hamiltonian instead of Eq. (9):

$$\mathcal{H}' = \mathcal{H}'_c + \lambda \mathcal{V}'_c, \tag{15}$$

with

$$\mathcal{H}'_c = \frac{J_1}{2} \sum_{i=1,2(\mathrm{mod}\,3)} D_1(i) + \frac{J_2}{2} \sum_{i=1(\mathrm{mod}\,3)} D_2(i) - H' \sum_j T^z_j, \tag{16}$$

$$\mathcal{V}'_c = \frac{J_1}{2} \sum_{i=0(\mathrm{mod}\,3)} D_1(i) + \frac{J_2}{2} \sum_{i=0,2(\mathrm{mod}\,3)} D_2(i), \tag{17}$$

where the ηth-neighbor two-spin (dimer) interaction is represented by $D_\eta(i) = T^+_i T^-_{i+\eta} + T^-_i T^+_{i+\eta} + T^z_i T^z_{i+\eta}$. $\mathcal{H}'_c$ ($\mathcal{V}'_c$) corresponds to the intracluster (intercluster) Hamiltonian denoted by the red (blue) lines in Fig. 4(a). We introduce the coupling strength λ to control the intercluster interactions. We note that Eq. (15) with $\lambda = 1$ is equivalent to Eq. (9).

A. Eigenstates of the magnetic unit cell

Since the Hamiltonian (16) does not include the interaction between the clusters, we can diagonalize it in each cluster. The resulting eigenstates $|\chi^{\pm}\rangle$ ($\chi = \alpha, \beta, \gamma$, and δ) are shown in Table I, with

$$C_{\pm} = \sqrt{\frac{1}{2}\left(1 \pm \frac{J_1 + J_2}{\sqrt{33J_1^2 + 2J_1J_2 + J_2^2}}\right)}. \tag{18}$$

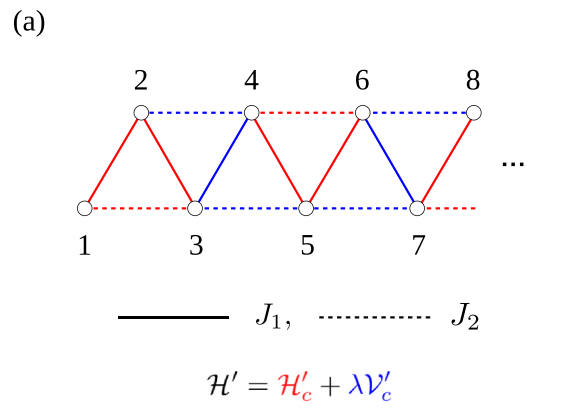

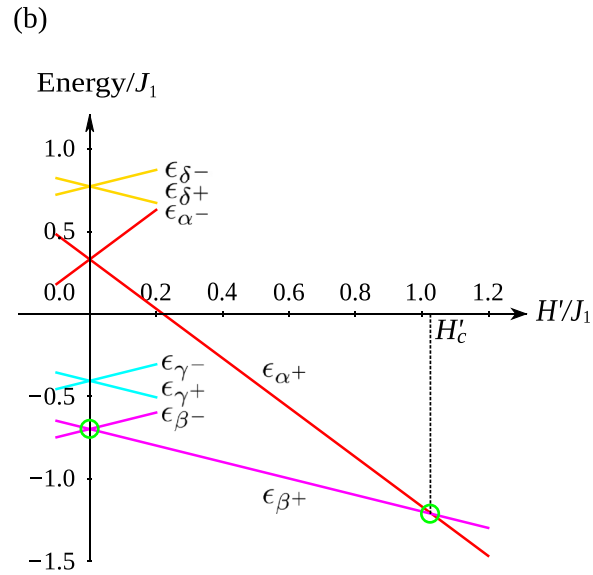

FIG. 4. (a) Clusterization based on spontaneously broken symmetry (CBSBS) of the AFSC. The numbers denote the quasispin site. The solid (dotted) lines correspond to J_1 (J_2) interactions. Red and blue lines are used to distinguish the intracluster Hamiltonian $\mathcal{H}'_c$ and intercluster Hamiltonian $\mathcal{V}'_c$, respectively. (b) Energy levels of local states $|\chi^{\pm}\rangle$ in effective magnetic fields H' in the case of $J_2/J_1 = 0.65$. The lowest-energy state encounters level crossing at $H' = 0$ and H'_c, denoted by the green circles.

The eigenenergy $\epsilon_{\chi^{\pm}}$ is given by

$$\epsilon_{\alpha^{\pm}} = \frac{1}{8}(2J_1 + J_2) \mp \frac{3}{2}H', \quad \epsilon_{\gamma^{\pm}} = -\frac{5}{8}J_2 \mp \frac{H'}{2}, \tag{19}$$

$$\epsilon_{\beta^{\pm}} = \frac{1}{8}\left(-J_1 + 2J_2 - \sqrt{33J_1^2 + 2J_1J_2 + J_2^2}\right) \mp \frac{H'}{2}, \tag{20}$$

$$\epsilon_{\delta^{\pm}} = \frac{1}{8}\left(-J_1 + 2J_2 + \sqrt{33J_1^2 + 2J_1J_2 + J_2^2}\right) \mp \frac{H'}{2}. \tag{21}$$

$|\chi^+\rangle$ and $|\chi^-\rangle$ correspond to a Kramers doublet due to the time-reversal symmetry when $H' = 0$. With the application of magnetic field, every Kramers doublet splits off, and degeneracy lifts [see Fig. 4(b)]. If interactions between the magnetic unit cells are completely classical and weaker than $\mathcal{H}'_c$, the ground state under the classical limit of intercluster interactions is given by the direct product of β^+ for $J_2/J_1 = 0.65$, as expected from Fig. 4(b). We note that the product

TABLE I. Eigenstates $|\chi^{\pm}\rangle$ ($\chi = \alpha, \beta, \gamma$, and δ) of $\mathcal{H}'_c$.

	Configuration
$\|\alpha^+\rangle$	$\|\uparrow\uparrow\uparrow\rangle$
$\|\beta^+\rangle$	$\frac{1}{\sqrt{2}}C_- \|\downarrow\uparrow\uparrow\rangle - C_+ \|\uparrow\downarrow\uparrow\rangle + \frac{1}{\sqrt{2}}C_- \|\uparrow\uparrow\downarrow\rangle$
$\|\gamma^+\rangle$	$-\frac{1}{\sqrt{2}}(\|\downarrow\uparrow\uparrow\rangle - \|\uparrow\uparrow\downarrow\rangle)$
$\|\delta^+\rangle$	$\frac{1}{\sqrt{2}}C_+ \|\downarrow\uparrow\uparrow\rangle + C_- \|\uparrow\downarrow\uparrow\rangle + \frac{1}{\sqrt{2}}C_+ \|\uparrow\uparrow\downarrow\rangle$
$\|\beta^-\rangle$	$\frac{1}{\sqrt{2}}C_- \|\uparrow\downarrow\downarrow\rangle - C_+ \|\downarrow\uparrow\downarrow\rangle + \frac{1}{\sqrt{2}}C_- \|\downarrow\downarrow\uparrow\rangle$
$\|\gamma^-\rangle$	$-\frac{1}{\sqrt{2}}(\|\uparrow\downarrow\downarrow\rangle - \|\downarrow\downarrow\uparrow\rangle)$
$\|\delta^-\rangle$	$\frac{1}{\sqrt{2}}C_+ \|\uparrow\downarrow\downarrow\rangle + C_- \|\downarrow\uparrow\downarrow\rangle + \frac{1}{\sqrt{2}}C_+ \|\downarrow\downarrow\uparrow\rangle$
$\|\alpha^-\rangle$	$\|\downarrow\downarrow\downarrow\rangle$

state describes the $m' = 1/3$ MP phase. In the following, we use this ground state as an approximated $m' = 1/3$ MP state, i.e., $|1/3\rangle \equiv \bigotimes_l |\beta^+\rangle_l$, where l denotes the cluster number.

In order to obtain dispersion relations of $T^{\pm}$ excitations, we use a semiclassical approximation of intercluster interactions in subsequent sections, where low-lying states in the cluster are taken into account in addition to the ground state.

B. T^+ excitation

To understand the T^+ excitation in the $m' = 1/3$ MP phase of the AFSC, we consider the fully spin polarized $|\alpha^+\rangle$ state as a low-lying state in the cluster because T^+ increases magnetization from the ground state $|1/3\rangle$. There are, of course, higher-order processes, including other excited states, e.g., a mixed state of two $|\alpha^+\rangle$ and one $|\beta^-\rangle$ in three magnetic unit cells, but such processes can be ignored because only two states, $|\alpha^+\rangle$ and $|\beta^+\rangle$, contribute to low-energy excitations around the critical field $H'_c = (3J_1 - J_2 + \sqrt{33J_1^2 + 2J_1J_2 + J_2^2})/8$, where $|\alpha^+\rangle$ and $|\beta^+\rangle$ are degenerate [see Fig. 4(b)]. Therefore, we use the projection to these two states, $\mathcal{Q}_+ = \prod_l (|\alpha^+\rangle_l \langle\alpha^+|_l + |\beta^+\rangle_l \langle\beta^+|_l)$. In the projected Hamiltonian, there is the constraint that $|\alpha^+\rangle_l \langle\alpha^+|_l + |\beta^+\rangle_l \langle\beta^+|_l = 1$. The operators $\tau_l^\dagger = |\alpha^+\rangle_l \langle\beta^+|_l$, $\tau_l = |\beta^+\rangle_l \langle\alpha^+|_l$, and $n_l = |\alpha^+\rangle_l \langle\alpha^+|_l$ correspond to hard-core bosonic creation, annihilation, and number operators, respectively. Thus, by using these operators with $\lambda = 1$, the projected Hamiltonian $\mathcal{H}''_+ = \mathcal{Q}_+\mathcal{H}'\mathcal{Q}_+$, except for the constant term, is given by

$$\mathcal{H}''_+ = t\sum_l (\tau_l^\dagger \tau_{l+1} + \text{H.c.}) + V\sum_l n_l n_{l+1} + \mu\sum_l n_l, \tag{22}$$

with

$$t = \tfrac{1}{4}C_-(J_1C_- - 2\sqrt{2}J_2C_+), \tag{23}$$

$$V = \tfrac{1}{8}[J_1C_-^4 + J_2(C_-^2 - C_+^2)^2], \tag{24}$$

$$\mu = \epsilon_{\beta^+} - \epsilon_{\alpha^+} - \tfrac{1}{4}(J_1C_-^2 + J_2C_+^2). \tag{25}$$

If we define the Fourier transform of the one-particle excited state as

$$|K\rangle = \sum_l e^{iKl} |\alpha^+\rangle_l \bigotimes_{l'(\neq l)} |\beta^+\rangle_{l'}, \tag{26}$$

this state is an eigenstate of the projected Hamiltonian $\mathcal{H}''_+$ with dispersion energy

$$\epsilon''_K = 2t\cos K + \text{const.} \tag{27}$$

This eigenstate represents the one-particle (hard-core boson) excited state obtained by the creation and annihilation operators, $\tau^\dagger$ and τ.

Analyzing the T^+ excitation in the $m' = 1/3$ MP phase of the AFSC, we use the relation $K = 3q_x$ because the periodicity of the AFSC is three times longer than that of the projected model (22). The white line in Fig. 2(c) exhibits the dispersion relation ϵ''_K including the constant energy in Eq. (27). The result reproduces well the dispersion relation of peak structure in the DSSF of the AFSC. This hard-core bosonic excitation is a collective mode of three-spin clusters (trimer), and thus, we call it a *trimeron* in this paper. Furthermore, as explained in Sec. III B, $T^+(q,\omega)$ in the $m' = 1/3$ MP phase is qualitatively equivalent to $S^-(q_x,\omega)$ in the $m = 1/3$ MP phase and $S^+(q_x,\omega)$ in the $m = 2/3$ MP phase of the FSL. We thus conclude that the origin of these DSSFs of the FSL is the trimeron, that is, one-particle excitation of the hard-core boson based on three-spin clusters.

C. T^- excitation

The T^- excitation in the $m' = 1/3$ MP phase of the AFSC is more difficult to understand than the T^+ excitation because we have to take several states into account as low-lying states of the cluster. However, our purpose in this section is to give an intuitive physical picture to explain the DSSF in Fig. 3(c). Hence, quantitative reproduction is not necessary. Here, we discuss the excitation through the CBSBS similar to the T^+ excitation. We consider three excited states, $|\beta^-\rangle$, $|\gamma^-\rangle$, and $|\delta^-\rangle$, as low-lying excited states of the cluster. If interactions between clusters do not exist, the DSSF shows local excitations corresponding to $|\beta^-\rangle$, $|\gamma^-\rangle$, and $|\delta^-\rangle$, which induce three flat bands. By adding the interactions as perturbation, the three bands become dispersive, indicating three modes of hard-core bosonic one-particle excitation (three trimerons) [see Fig. 5(a)]. When the energy scale of interactions is larger than energy gaps between three excited states, theses modes are hybridized and split off.

Figure 5 shows the λ dependence of $T^-(q,\omega)$ in the effective model (15) for the $m' = 1/3$ MP phase of AFSC. Note that Fig. 5(c) (the case of $\lambda = 1$) is the same as Fig. 3(c). In Fig. 5 we also plots dispersion relations of three modes, $|\beta^-\rangle$, $|\gamma^-\rangle$, and $|\delta^-\rangle$, which is obtained from the projected Hamiltonian $\mathcal{H}''_- = \mathcal{Q}_-\mathcal{H}'\mathcal{Q}_-$, with $\mathcal{Q}_- = \prod_l (|\beta^+\rangle_l \langle\beta^+|_l + \sum_{\chi=\beta,\gamma,\delta} |\chi^-\rangle_l \langle\chi^-|_l)$ but neglecting hybridization among the three modes for simplicity. From Fig. 5(c), we can easily imagine that, if we introduce the hybridization effect, the β^- and γ^- modes would be repulsively separated more around $q = 2\pi/3$ and the γ^--originated mode would construct the lowest-energy excitations around $q = 2\pi/3$ that are seen in $T^-(q,\omega)$. This speculation based on hybridized trimerons will explain the change in spectral distribution from $\lambda = 1$ to $\lambda = 0.5$, where the splitting of spectral weight around $q = 2\pi/3$ disappears with decreasing λ because of the reduction of intercluster interactions controlling the hybridization of trimerons.

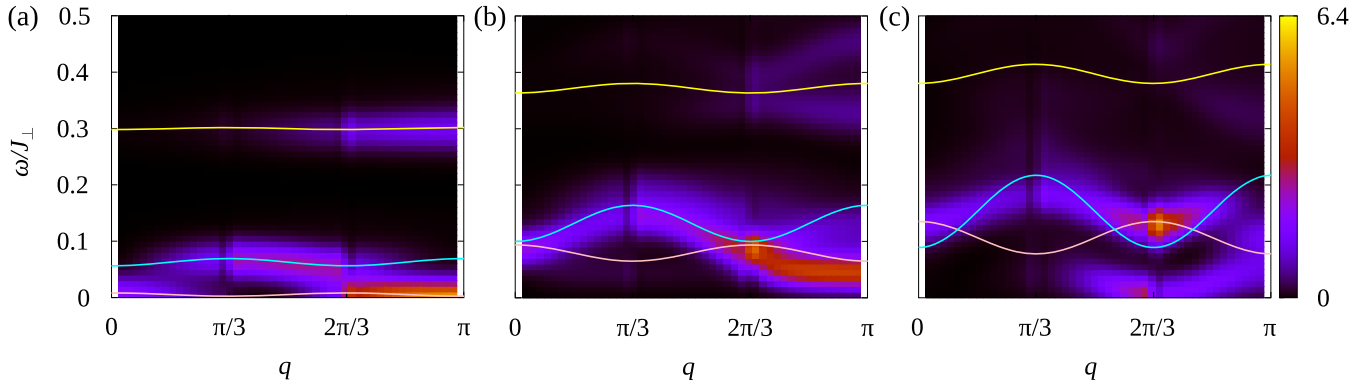

FIG. 5. $T^-(q,\omega)$ in the effective model (15) for the $m' = 1/3$ MP phase of the AFSC with various coupling ratios: (a) $\lambda = 0.1$, (b) $\lambda = 0.5$, and (c) $\lambda = 1.0$. The dispersion relations in pink, blue, and yellow indicate the β^-, γ^-, and δ^- modes, respectively, in the projected Hamiltonian $\mathcal{H}''_-$ without hybridization among these modes.

Based on these considerations in this section and Sec. IV B, we conclude that $S^+(q_x,\omega)$ in the $m = 1/3$ MP phase and $S^-(q_x,\omega)$ in the $m = 2/3$ MP phase of the FSL originate from the hybridized trimerons.

V. SUMMARY

In this paper, we have studied magnetic excitations in the MP phases of the FSL, where the three types of antiferromagnetic interactions, J_1, J_2 and $J_\perp$, are taken into account as the leg nearest-neighbor, leg second-neighbor, and rung nearest-neighbor couplings of a two-leg ladder, respectively. This model exhibits three MPs at fractionalized finite magnetization $m = M/M_{\rm sat} = 1/3$, $1/2$, and $2/3$ with respect to saturation magnetization $M_{\rm sat}$. These MPs emerge robustly in the strong-rung limit. Moreover, this condition allows us to map the model Hamiltonian into another quasispin model, the AFSC, by ignoring high-energy states in a rung. To obtain the intuitive physical picture of spin dynamics through the mapping to the AFSC, we have focused on the strong-rung range.

We first obtained magnetic excitations of the FSL by calculating DSSFs using the DDMRG method. We have found that magnetic excitations in the MP phase are commensurate to the enlarged unit cell of the MP ground state. For the sake of comparison, we have also calculated DSSFs in the AFSC of quasispins and have confirmed that the AFSC reproduces low-energy excitations of the FSL qualitatively. The $m = 1/3$, $1/2$, and $2/3$ MP states in the FSL correspond to the $m' = -1/3$, 0, and $1/3$ MP states in the AFSC, respectively. The zero-magnetization ground state of the AFSC is well known as the dimerized state, so that elementary excitations are regarded as bound spinons. Therefore, we conclude that low-energy magnetic excitations of the FSL correspond to bound quasispinons based on the singlet and + triplet states of the rung.

To clarify the S^+ (S^-) excitation in the $m = 2/3$ $(1/3)$ MP state, we have additionally analyzed spin dynamics through the CBSBS in the AFSC. In the CBSBS, one cluster corresponds to an enlarged unit cell after spontaneously breaking translational symmetry, and intercluster interactions are treated as perturbative effects compared with the intracluster interaction. We have found a quasiparticle mode that is a hard-core bosonic excitation in the $m = 1/3$ MP state of the AFSC, which we call a trimeron because it is a collective mode of spin trimers. This trimeron picture is common to the S^+ (S^-) excitation in the $m = 2/3$ $(1/3)$ MP state of the FSL. On the other hand, the S^- (S^+) excitation in the $m = 2/3$ $(1/3)$ MP state is not well described as a single trimeron mode. We have thus examined the intracluster interaction dependence of the DSSF. The obtained result indicates that intermode coupling enhanced by the intercluster interactions is crucial even for low-energy excitation. Actually, we have confirmed that two low-lying modes are hybridized in the excitation spectra with increasing the intercluster interactions, which are regarded as a hybridized trimerons. Consequently, we conclude that the S^- (S^+) excitation in the $m = 2/3$ $(1/3)$ MP state corresponds to the hybridized trimerons of quasi-spins.

Our results will be useful for understanding the low-energy physics in not only FSL materials such as $BiCu_2PO_6$ [13–16] and $Li_2Cu_2O(SO_4)_2$ [17–20] but also weakly coupled spin dimer compounds [43–45], where magnetic excitations originating from the identified quasiparticle can be clarified by inelastic neutron scattering experiments in a magnetic field. In such materials, we have clarified that spin dynamics is also important for understanding the spin or heat transport [27–29], including their application to spintronics [9,10]. Furthermore, the CBSBS is also useful for the analyses of low-energy excitations in MPs of various spin systems. We expect that new quasiparticle N-merons will be discovered as elementary excitations in the MPs, where the enlarged unit cell includes N original cells after spontaneous breaking of translational symmetry.

ACKNOWLEDGMENTS

We would like to thank H. Onishi, M. Mori, S. Maekawa, and K. Okamoto for fruitful discussions. This work was partly supported by the creation of new functional devices and high-performance materials to support next- generation industries (CDMSI) to be tackled by using a post-K computer, Grants-in-Aid for Young Scientists (B) (Grant No. 16K17753), and the inter-university cooperative research program of IMR, Tohoku University. Numerical computation in this work was

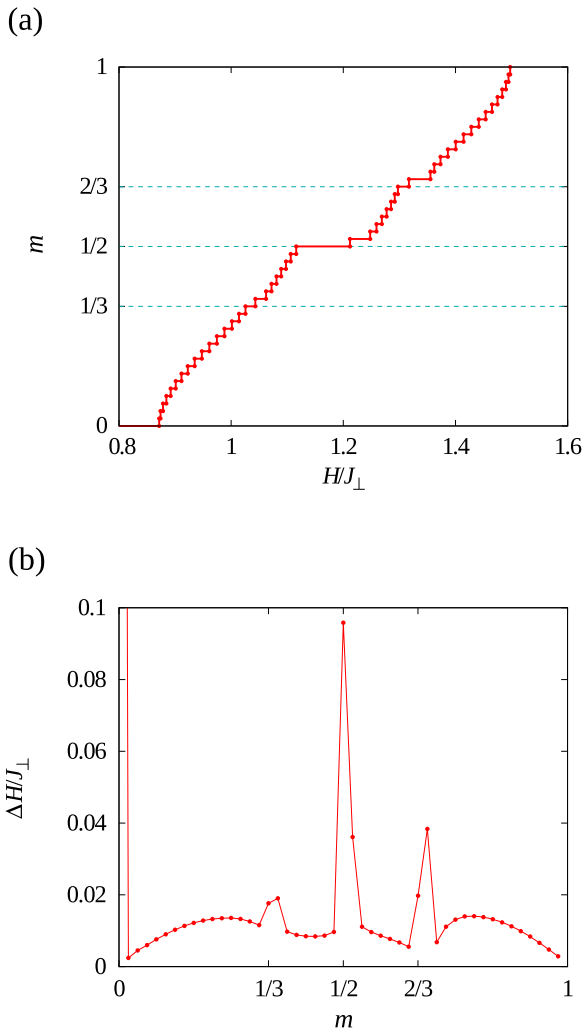

FIG. 6. (a) Magnetization curves normalized by saturation magnetization, $m = M(H)/M_{\rm sat}$, for the 48-rung FSL with $J_1/J_\perp = 0.2$, $J_2/J_1 = 0.65$. (b) Field width ΔH as a function of magnetization m. The number of kept states in the DMRG is up to 500, and the truncation error is less than 10^{-9}.

carried out on the Supercomputer Center at Institute for Solid State Physics, University of Tokyo and the supercomputers at JAEA.

APPENDIX A: MAGNETIZATION CURVE

The DDMRG method usually requires numerous calculation resources compared with the DMRG method for the ground state. As a consequence, the system size for the DDMRG is smaller than that for the DMRG. In this paper, the system size of the FSL is set to be 48 rungs for the DDMRG, in contrast to the system with 72 rungs [11] and 144 rungs [12] for the DMRG. Small system size prevents us from three clear MPs, but we have managed to find them with an appropriate parameter set by calculating the magnetization curve in the 48-rung FSL with the DMRG method.

Figure 6(a) shows magnetization curves with $J_1/J_\perp = 0.2$ and $J_2/J_1 = 0.65$ in the 48-rung FSL. Here, by using the Heaviside step function $\theta(H)$, the magnetization curve is given by

$$M(H) = \sum_{M=1}^{M_{\rm sat}-1} M\theta(H - H_{M-1,M})\theta(H_{M,M+1} - H), \quad \text{(A1)}$$

and the magnetic field where the ground states with two different magnetizations M and $M+1$ are degenerate is obtained by $H_{M,M+1} \equiv E_{M+1} - E_M$, with the ground state energies E_M and E_{M+1} calculated by the DMRG method. To confirm the presence of three MPs, we check the field width $\Delta H(M) = E_{M+1} - E_M$ at magnetization M [see Fig. 6(b)]. If the ground state with M is gapless with respect to the S^+ excitation, the field width converges to zero in the thermodynamical limit. In Fig. 6(b), we can see three jumps at $m = 1/3$, $1/2$, and $2/3$, indicating the presence of three MPs. Therefore, we use this parameter set to calculate the DSSFs in this paper.

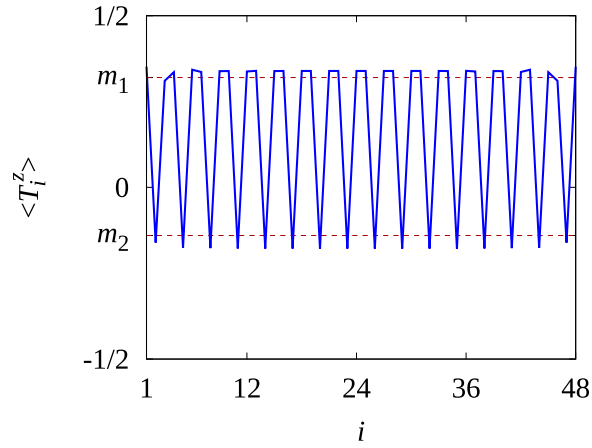

FIG. 7. Real-space expectation value of the z component of quasispin T_i^z in the $m' = 1/3$ MP phase. The red dashed lines denote $m_1 = \langle\beta^+|T_1^z|\beta^+\rangle = \langle\beta^+|T_3^z|\beta^+\rangle$ and $m_2 = \langle\beta^+|T_2^z|\beta^+\rangle$. The β^+ state is the ground state in the one-cluster (three quasispins) Hamiltonian (see Table I).

APPENDIX B: MAGNETIC STRUCTURE IN THE $m' = \frac{1}{3}$ MP PHASE OF THE ASFC

In Sec. IV, we use the CBSBS to explain the DSSFs in the $m' = 1/3$ MP phase. Although large energy gaps with $m = 1/3$ and $2/3$ are confirmed even in the 48-rung FSL, it is unclear whether the spin configuration shows symmetry breaking with a three times larger unit cell in the 48-site AFSC. To confirm the enlarged magnetic unit cell in the ASFC, we calculate the expectation value of the z component of quasispin T_i^z in the $m' = 1/3$ MP phase as shown in Fig. 7. The period is found to be three times longer than the original unit cell. Moreover, the expectation values are approximately equivalent to $m_1 = \langle\beta^+|T_1^z|\beta^+\rangle = \langle\beta^+|T_3^z|\beta^+\rangle$ and $m_2 = \langle\beta^+|T_2^z|\beta^+\rangle$, which are estimated in the ground state in the one-cluster (three quasispins) Hamiltonian. This result also supports the CBSBS approach.

[1] For a review for the spin liquid, see L. Balents, Nature (London) **464**, 199 (2010).

[2] For a theoretical study on magnetization plateaus, see M. Oshikawa, M. Yamanaka, and I. Affleck, Phys. Rev. Lett. **78**, 1984 (1997).

[3] As an alternative to the theoretical study [2], see K. Totsuka, Phys. Rev. B **57**, 3454 (1998).

[4] For an experimental study on magnetization plateaus, see H. Kageyama, K. Yoshimura, R. Stern, N. V. Mushnikov, K. Onizuka, M. Kato, K. Kosuge, C. P. Slichter, T. Goto, and Y. Ueda, Phys. Rev. Lett. **82**, 3168 (1999).

[5] K. Okunishi and T. Tonegawa, J. Phys. Soc. Jpn. **72**, 479 (2003); Phys. Rev. B **68**, 224422 (2003).

[6] T. Hong, M. Matsumoto, Y. Qiu, W. Chen, T. R. Gentile, S. Watson, F. F. Awwadi, M. M. Turnbull, S. E. Dissanayake, H. Agrawal, R. Toft-Petersen, B. Klemke, K. Coester, K. P. Schmidt, and D. A. Tennant, Nat. Phys. **13**, 638 (2017).

[7] T. Hong, Y. Qiu, M. Matsumoto, D. A. Tennant, K. Coester, K. P. Schmidt, F. F. Awwadi, M. M. Turnbull, H. Agrawal, and A. L. Chernyshev, Nat. Commun. **8**, 15148 (2017).

[8] T. Ying, K. P. Schmidt, and S. Wessel, Phys. Rev. Lett. **122**, 127201 (2019).

[9] K. Uchida, S. Takahashi, K. Harii, J. Ieda, W. Koshibae, K. Ando, S. Maekawa, and E. Saitoh, Nature (London) **455**, 778 (2008).

[10] D. Hirobe, M. Sato, T. Kawamata, Y. Shiomi, K. Uchida, R. Iguchi, Y. Koike, S. Maekawa, and E. Saitoh, Nat. Phys. **13**, 30 (2017).

[11] T. Sugimoto, M. Mori, T. Tohyama, and S. Maekawa, Phys. Rev. B **92**, 125114 (2015).

[12] T. Sugimoto, M. Mori, T. Tohyama, and S. Maekawa, Phys. Rev. B **97**, 144424 (2018).

[13] F. Abraham, M. Ketatni, G. Mairesse, and B. Mernari, Eur. J. Solid State Inorg. Chem. **31**, 313 (1994).

[14] B. Koteswararao, S. Salunke, A. V. Mahajan, I. Dasgupta, and J. Bobroff, Phys. Rev. B **76**, 052402 (2007).

[15] O. Mentré, E. Janod, P. Rabu, M. Hennion, F. Leclercq-Hugeux, J. Kang, C. Lee, M.-H. Whangbo, and S. Petit, Phys. Rev. B **80**, 180413(R) (2009).

[16] A. A. Tsirlin, I. Rousochatzakis, D. Kasinathan, O. Janson, R. Nath, F. Weickert, C. Geibel, A. M. Lauchli, and H. Rosner, Phys. Rev. B **82**, 144426 (2010).

[17] G. Rousse, J. Rodríguez-Carvajal, C. Giacobbe, M. Sun, O. Vaccarelli, and G. Radtke, Phys. Rev. B **95**, 144103 (2017).

[18] M. Sun, G. Rousse, A. M. Abakumov, M. Saubanère, M.-L. Doublet, J. Rodríguez-Carvajal, G. Van Tendeloo, and J.-M. Tarascon, Chem. Mater. **27**, 3077 (2015).

[19] O. Vaccarelli, G. Rousse, A. Saúl, and G. Radtke, Phys. Rev. B **96**, 180406(R) (2017).

[20] O. Vaccarelli, A. Honecker, P. Giura, K. Béneut, B. Fåk, G. Rousse, and G. Radtke, Phys. Rev. B **99**, 064416 (2019).

[21] Y. Kohama, S. Wang, A. Uchida, K. Prsa, S. Zvyagin, Y. Skourski, R. D. McDonald, L. Balicas, H. M. Ronnow, C. Rüegg, and M. Jaime, Phys. Rev. Lett. **109**, 167204 (2012).

[22] F. Casola, T. Shiroka, A. Feiguin, S. Wang, M. S. Grbić, M. Horvatić, S. Krämer, S. Mukhopadhyay, K. Conder, C. Berthier, H.-R. Ott, H. M. Rønnow, C. Rüegg, and J. Mesot, Phys. Rev. Lett. **110**, 187201 (2013).

[23] Y. Kohama, K. Mochidzuki, T. Terashima, A. Miyata, A. DeMuer, T. Klein, C. Marcenat, Z. L. Dun, H. Zhou, G. Li, L. Balicas, N. Abe, Y. H. Matsuda, S. Takeyama, A. Matsuo, and K. Kindo, Phys. Rev. B **90**, 060408(R) (2014).

[24] M. Colmont, C. Darie, A. A. Tsirlin, A. Jesche, C. Colin, and O. Mentré, Inorg. Chem. **57**, 6038 (2018).

[25] K. W. Plumb, Z. Yamani, M. Matsuda, G. J. Shu, B. Koteswararao, F. C. Chou, and Y.-J. Kim, Phys. Rev. B **88**, 024402 (2013).

[26] K. W. Plumb, K. Hwang, Y. Qiu, L. W. Harriger, G. E. Granroth, A. I. Kolesnikov, G. J. Shu, F. C. Chou, C. Rüegg, Y. B. Kim, and Y.-J. Kim, Nat. Phys. **12**, 224 (2016).

[27] H. Nagasawa, T. Kawamata, K. Naruse, M. Ohno, Y. Matsuoka, H. Sudo, Y. Hagiya, M. Fujita, T. Sasaki, and Y. Koike, J. Phys.: Conf. Ser. **568**, 042012 (2014).

[28] B.-G. Jeon, B. Koteswararao, C. B. Park, G. J. Shu, S. C. Riggs, E. G. Moon, S. B. Chung, F. C. Chou, and K. H. Kim, Sci. Rep. **6**, 36970 (2016).

[29] T. Kawamata, H. Nagasawa, K. Naruse, M. Ohno, Y. Matsuoka, Y. Hagiya, M. Fujita, T. Sasaki, and Y. Koike, J. Phys. Soc. Jpn. **87**, 074702 (2018).

[30] A. Lavarélo, G. Roux, and N. Laflorencie, Phys. Rev. B **84**, 144407 (2011).

[31] T. Sugimoto, M. Mori, T. Tohyama, and S. Maekawa, Phys. Rev. B **87**, 155143 (2013).

[32] I. T. Shyiko, I. P. McCulloch, J. V. Gumenjuk-Sichevska, and A. K. Kolezhuk, Phys. Rev. B **88**, 014403 (2013).

[33] L. Splinter, N. A. Drescher, H. Krull, and G. S. Uhrig, Phys. Rev. B **94**, 155115 (2016).

[34] K. Hwang and Y. B. Kim, Phys. Rev. B **93**, 235130 (2016).

[35] S. R. White, Phys. Rev. Lett. **69**, 2863 (1992); Phys. Rev. B **48**, 10345 (1993).

[36] E. Jeckelmann, Phys. Rev. B **66**, 045114 (2002).

[37] U. Schollwöck, Rev. Mod. Phys. **77**, 259 (2005).

[38] S. Sota and T. Tohyama, Phys. Rev. B **82**, 195130 (2010).

[39] S. Sachdev and R. N. Bhatt, Phys. Rev. B **41**, 9323 (1990).

[40] T. Giamarchi and A. M. Tsvelik, Phys. Rev. B **59**, 11398 (1999).

[41] A. Lavarélo and G. Roux, Eur. Phys. J. B **87**, 229 (2014).

[42] For the isotropic case of spin interactions, see K. Okunishi and T. Tonegawa, J. Phys. Soc. Jpn. **74**, 151 (2005).

[43] K. Kodama, M. Takigawa, M. Horvatić, C. Berthier, H. Kageyama, Y. Ueda, S. Miyahara, F. Becca, and F. Mila, Science **298**, 395 (2002).

[44] Ch. Rüegg, N. Cavadini, A. Furrer, H.-U. Güdel, K. Krämer, H. Mutka, A. Wildes, K. Habicht, and P. Vorderwisch, Nature (London) **423**, 62 (2003).

[45] S. Kimura, K. Kakihata, Y. Sawada, K. Watanabe, M. Matsumoto, M. Hagiwara, and H. Tanaka, Nat. Commun. **7**, 12822 (2016).